

Global properties of K hindrance probed by the gamma decay of the warm rotating W-174 nucleus

V. Vandone, S. Leoni, G. Benzoni, N. Blasi, A. Bracco, S. Brambilla, C. Boiano, S. Bottoni, F. Camera, A. Corsi, et al.

▶ **To cite this version:**

V. Vandone, S. Leoni, G. Benzoni, N. Blasi, A. Bracco, et al.. Global properties of K hindrance probed by the gamma decay of the warm rotating W-174 nucleus. Physical Review C, American Physical Society, 2013, 88, pp.034312. 10.1103/PhysRevC.88.034312 . in2p3-00916808

HAL Id: in2p3-00916808
http://hal.in2p3.fr/in2p3-00916808

Submitted on 31 May 2021

HAL is a multi-disciplinary open access archive for the deposit and dissemination of scientific research documents, whether they are published or not. The documents may come from teaching and research institutions in France or abroad, or from public or private research centers.

L'archive ouverte pluridisciplinaire **HAL**, est destinée au dépôt et à la diffusion de documents scientifiques de niveau recherche, publiés ou non, émanant des établissements d'enseignement et de recherche français ou étrangers, des laboratoires publics ou privés.

Global properties of K hindrance probed by the γ decay of the warm rotating ^{174}W nucleus

V. Vandone,[1,2] S. Leoni,[1,2,*] G. Benzoni,[2] N. Blasi,[2] A. Bracco,[1,2] S. Brambilla,[2] C. Boiano,[2] S. Bottoni,[1,2] F. Camera,[1,2] A. Corsi,[1,2,†] F. C. L. Crespi,[1,2] A. Giaz,[1,2] B. Million,[2] R. Nicolini,[1,2] L. Pellegri,[1,2] A. Pullia,[1,2] O. Wieland,[2] D. Bortolato,[3] G. de Angelis,[3] E. Calore,[3] A. Gottardo,[3] G. Maron,[3] D. R. Napoli,[3] D. Rosso,[3] E. Sahin,[3] J. J. Valiente-Dobon,[3] D. Bazzacco,[4] M. Bellato,[4,5] E. Farnea,[4] S. Lunardi,[4,5] R. Menegazzo,[4,5] D. Mengoni,[4,5,6] P. Molini,[4,5] C. Michelagnoli,[4,5] D. Montanari,[4,5] F. Recchia,[4,5] C. A. Ur,[4] A. Gadea,[7] T. Hüyük,[7] N. Cieplicka,[8] A. Maj,[8] M. Kmiecik,[8] A. Atac,[9] S. Akkoyun,[9,‡] A. Kaskas,[9] P.-A. Söderström,[10] B. Birkenbach,[11] B. Cederwall,[12] P. J. Coleman-Smith,[13] D. M. Cullen,[14] P. Désesquelles,[15] J. Eberth,[11] A. Görgen,[16,17] J. Grebosz,[8] H. Hess,[11] D. Judson,[18] A. Jungclaus,[19] N. Karkour,[15] P. Nolan,[18] A. Obertelli,[16] P. Reiter,[11] M. D. Salsac,[16] O. Stezowski,[20] Ch. Theisen,[16] M. Matsuo,[21] and E. Vigezzi[2]

[1]*Dipartimento di Fisica, Università di Milano, I-20133 Milano, Italy*
[2]*INFN, Sezione di Milano via Celoria 16, I-20133 Milano, Italy*
[3]*INFN, Laboratori Nazionali di Legnaro, I-35020 Legnaro (PD), Italy*
[4]*INFN, Sezione di Padova, I-35131 Padova, Italy*
[5]*Dipartimento di Fisica e Astronomia dell' Università di Padova, I-35131 Padova, Italy*
[6]*School of Engineering, University of West Scotland, Paisley PA1 2BE, United Kingdom*
[7]*IFIC, CSIC-University of Valencia, Valencia, Spain*
[8]*The Henryk Niewodniczań ski Institute of Nuclear Physics, Polish Academy of Sciences, 31-342 Kraków, Poland*
[9]*Department of Physics, Faculty of Science, Ankara University, Ankara, Turkey*
[10]*Department of Physics and Astronomy, Uppsala University, Sweden*
[11]*Institut für Kernphysik, Universität zu Köln, Zülpicher Str. 77, D-50937 Köln, Germany*
[12]*Department of Physics, Royal Institute of Technology, SE-10691 Stockholm, Sweden*
[13]*STFC Daresbury Laboratory, Daresbury, Warrington WA4 4AD, United Kingdom*
[14]*Nuclear Physics Group, Schuster Laboratory, University of Manchester, Manchester M13 9PL, United Kingdom*
[15]*CSNSM, CNRS/IN2P3 and Univ. Paris-Sud, F-91405 Orsay Campus, France*
[16]*IRFU, CEA/DSM, Centre CEA de Saclay, F-91191 Gif-sur-Yvette Cedex, France*
[17]*Department of Physics, University of Oslo, P. O. Box 1048 Blindern, N-0316 Oslo, Norway*
[18]*Oliver Lodge Laboratory, The University of Liverpool, Liverpool L69 7ZE, United Kingdom*
[19]*Instituto de Estructura de la Materia, CSIC, Madrid, E-28006 Madrid, Spain*
[20]*Université de Lyon, F-69622, Lyon, France; Université Lyon 1, Villeurbanne; and CNRS/IN2P3, UMR5822, IPNL*
[21]*Graduate School of Science and Technology, Niigata University, Niigata 950-2181, Japan*

(Received 26 July 2013; published 13 September 2013)

The K hindrance to the γ decay is studied in the warm rotating ^{174}W nucleus, focusing on the weakening of the selection rules of the K quantum number with increasing excitation energy. ^{174}W was populated by the fusion reaction of ^{50}Ti (at 217 MeV) on a ^{128}Te target, and its γ decay was detected by the AGATA Demonstrator array coupled to a BaF_2 multiplicity filter at Laboratori Nazionali di Legnaro of INFN. A fluctuation analysis of γ coincidence matrices gives a similar number of low-K and high-K discrete excited bands. The results are compared to simulations of the γ-decay flow based on a microscopic cranked shell model at finite temperature in which the K mixing is governed by the interplay of Coriolis force with the residual interaction. Agreement between simulations and experiment is obtained only by hindering the $E1$ decay between low-K and high-K bands by an amount compatible with that determined by spectroscopic studies of K isomers in the same mass region, with a similar trend with excitation energy. The work indicates that K mixing due to temperature effects may play a leading role for the entire body of discrete excited bands, which probes the onset region of K weakening.

DOI: 10.1103/PhysRevC.88.034312 PACS number(s): 21.10.Re, 23.20.Lv, 21.60.Ev, 27.70.+q

I. INTRODUCTION

Investigations of nuclear isomerisms have played an important part in the development of modern ideas about atomic nuclei. The long half-lives of isomeric states favor the study of the structure of the nucleus, in particular at the limit of nuclear stability, and have astrophysical implications and offer a number of practical applications, including medical diagnostics and energy storage [1–3]. In spite of remarkable advances in the experimental investigation, a quantitative theory of decay transition rates remains difficult [4,5] and largely depends on the specific kind of isomerism, either related to a shape change (shape isomer) [6] or to large change in spin or in its orientation (spin trap or K trap, respectively) [3].

*Corresponding author: silvia.leoni@mi.infn.it
†Present address: CEA, Centre de Saclay, IRFU/Service de Physique Nucleaire, F-91191 Gif-sur-Yvette, France.
‡Present address: Department of Physics, Faculty of Science, Cumhuriyet University, Sivas, Turkey.

 ©2013 American Physical Society

In axially deformed symmetric systems, away from closed shells, K isomers are the most abundant, K being the projection of the nuclear angular momentum on the symmetry axis of the nucleus. Their existence arises from the approximate conservation of K: In an electromagnetic de-excitation, if K were a good quantum number, the change in K should not exceed λ, the transition multipole order. Transitions that violate this rule are called K forbidden. In reality, rather than strictly forbidden, such transitions are strongly hindered, resulting in long-lived isomeric states. Empirically, it was found in early studies that the associated transition rates depend on the degree of forbiddenness, $\nu = \Delta K - \lambda$, and that for each extra unit of forbiddenness the transition rate is typically slowed down by the so-called reduced hindrance factor $f_\nu = (F_w)^{1/\nu} \approx 100$, F_w being the ratio of the Weisskopf estimate to the measured transition rates [7]. This empirical rule was at least qualitatively interpreted within perturbation theory in terms of the Coriolis mixing with a fixed axial shape [8]. Subsequent studies of K isomers in the mass region $A \approx 160$–180 have, however, shown that the reduced hindrance factors f_ν can assume remarkably smaller values, as compared to the empirical rule [1,9], and several direct decays to the $K = 0$ band have been observed. Different theoretical mechanisms have been proposed to explain these abnormally fast decays. The possibility of coupling to collective triaxial states was proposed early [10,11], and systematic calculations of collective tunneling in the γ degree of freedom [12] could successfully reproduce many, although not all, observed lifetimes of direct decay to the ground-state band [13,14]. Tunneling in the spin orientation has been proposed as an alternative mechanism, more suitable to explain decay to bands having intermediate values of K [15]. Finally, a systematic decline in reduced hindrance values is also observed with increasing internal energy U, i.e., the excitation energy of the isomeric state relative to the rotational energy at the same spin, and an interpretation based on statistical mixing among states having different K values, governed by the density of states, was proposed [1,16].

Until now, the relative importance of the various processes mentioned above remains unclear, resulting in large uncertainties in half-life predictions. Therefore, it becomes crucial to achieve a more comprehensive picture of the K-mixing phenomenon by gathering, for example, complementary information from the decay properties of the entire body of discrete excited high-K bands. This is done in the present work by the analysis of quasicontinuum spectra of γ rays emitted at high spins and high internal energy, probing the γ-decay feeding into specific low-lying configurations. A first example of this type of study was carried out in the nucleus ^{163}Er, in which the properties of γ-decay fluxes feeding low-K and high-K rotational bands have been exploited to probe the progressive weakening of selection rules on K with increasing internal energy U, focusing on the transition between order and chaos in a quantum-mechanical system [17–20].

In this paper we present results from an experiment performed with the AGATA Demonstrator, which represents the first phase of the Advanced GAmma Tracking Array [21,22]. The work aims at contributing to a global understanding of the K-hindrance phenomenon as a function of excitation energy by looking at the average properties of γ-decay fluxes in ^{174}W, populating quasicontinuum γ-γ coincidence spectra. This nucleus is characterized by the existence of a number of low-K bands ($K \leqslant 6$) extending up to spin $39\,\hbar$ and by three high-K rotational structures ($K \geqslant 8$), two of which ($K^\pi = 8^-$ and 12^+) were built on isomeric states with lifetimes longer than 120 ns [14,23]. In particular, the 12^+ isomer represents a peculiarity in the mass region $A \approx 180$, since its decay probability deviates strongly from the prediction by a γ-tunneling model, which accounts for the majority of isomeric decays in neighboring systems [12,14]. The present data are analysed in terms of event fluctuations, a well-established *ad hoc* technique [20,24] that makes it possible to carry out a quantitative investigation of rotational quasicontinuum spectra. The experimental results, in terms of number of discrete excited bands of low-K and high-K nature, are interpreted via a simulation of the collective γ decay, based on microscopic cranked shell model (CSM) calculations at finite temperature [25,26]. This is a powerful tool to quantitatively describe nuclear structure properties of warm rotating nuclei, probing key aspects of their γ decay, as previously done in different regions of mass and deformation [20,27–31]. It is anticipated that agreement between data and theory is obtained only by strongly quenching the decay strength of $E1$ statistical transitions between low-K and high-K discrete excited bands, resulting in reduced hindrance factors which follow the same trend, with excitation energy, as observed in spectroscopic studies of K isomers in the $A \approx 160$–180 mass region [9,16].

The paper is organized as follows. Section II describes the experimental setup, the employed reaction and the first steps of the data analysis. Details of the statistical analysis of quasicontinuum spectra associated to low-K and high-K structures are given in Sec. III. The Monte Carlo simulation used to interpret the experimental results is extensively discussed in Sec. IV, together with the cranking calculations which provide the microscopic input for the modeling of the γ-decay flow. Conclusions are given in Sec. V.

II. THE EXPERIMENT

The experiment was performed at Laboratori Nazionali di Legnaro (LNL) of Istituto Nazionale di Fisica Nucleare (INFN), Italy. A ^{50}Ti beam, provided by the TANDEM accelerator with an energy of 217 MeV, impinged on a ^{128}Te target (1 mg/cm^2 thick, backed by 50 mg/cm^2 of $^{\text{nat}}$Pb). This fusion reaction populates mainly ^{174}W and ^{173}W, with relative intensity of the order of 40% and 50%, respectively. According to PACE4 calculations [32], states up to $\sim 60\,\hbar$ and excitation energy of several MeV above yrast are reached, therefore providing a good population of the warm rotational regime. The experimental setup consisted of four triple clusters of the AGATA tracking array [21,22], placed at 16 cm from the target (with an absolute efficiency of $\sim$5% at 1.3 MeV), coupled to a multiplicity filter of 27 BaF_2 scintillator detectors (named HELENA), covering $\sim$25% of the total solid angle. The experiment was performed with an average current of 1 pnA to prevent target damage, requiring fourfold events in AGATA or threefold events in AGATA in coincidence with at least one event in HELENA, as trigger conditions. This

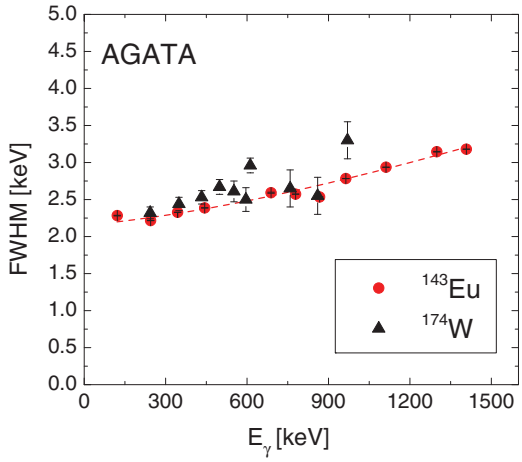


FIG. 1. (Color online) Full width at half maximum (FWHM) as a function of γ-ray energy, as obtained for the entire AGATA array from an ^{143}Eu source (circles) and the ground-state band of ^{174}W, populated in-beam in the present reaction (triangles). The dashed line is a linear fit of the ^{143}Eu source data.

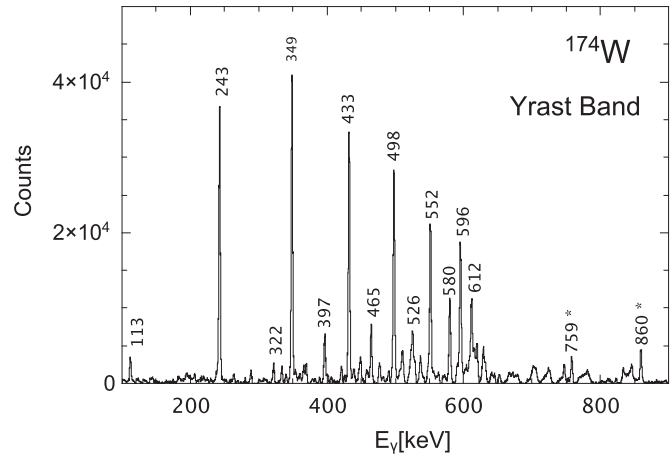


FIG. 2. γ spectrum obtained by gating on the lowest spin transitions of the four yrast band of ^{174}W. Energies are given for the yrast band and the strongly populated negative-parity band, labeled 4 in Ref. [14]. Stars mark interconnecting transitions.

resulted in event rates of ≈15 and 45 kHz in individual AGATA and HELENA detectors, giving rise to 4.5 kHz of triggered events.

The AGATA detectors were calibrated up to 9 MeV using an AmBe(Ni) source, while ^{88}Y was used for a low-energy calibration of the scintillators spectra. Time spectra were constructed and aligned for each HPGe and BaF_2 detector (the first as differences between the 12 AGATA detectors, the latter with respect to the trigger signal), resulting in a very similar time structure, with a time resolution of the order of 20 ns. Finally, a tracking algorithm [33] was applied to recover Compton scattering events and to improve the peak-to-background ratio of the AGATA array. This resulted in a Ge-fold distribution peaked around $F_\gamma(\text{AGATA}) = 2$. Due to the use of a backed target, no Doppler correction was further needed: as shown in Fig. 1, the full width at half maximum (FWHM) as a function of γ-ray energy (for the entire AGATA array) is very similar for source and in-beam data. In particular, a peak width of ≈2.5–3 keV is obtained at 0.6–1.2 MeV, which motivates the standard binning to 4 keV/ch used in the subsequent analysis of quasicontinuum γ-γ spectra, discussed in Sec. III.

By looking at sum-energy versus fold distributions measured in HELENA (in coincidence with low spin transitions of ^{174}W and ^{173}W), the fold condition $F_\gamma(\text{HELENA}) \geqslant 4$ was chosen to favor the selection of high-spin cascades, where the majority of the warm rotational flow of ^{174}W goes. The data were then sorted into γ-γ matrices collecting the population of low-K and high-K structures of ^{174}W separately, in order to investigate their properties and correlations through $E1$ γ decays. Five γ-γ coincidence spectra selecting the decay flow through the strongest low-K bands (labeled 1, 2, 3, 4, and 6 in Refs. [14,23]) were constructed by setting gates on clean transitions in the spin range ≈16–38 $\hbar$, in addition to a narrow gate on the prompt peak in the HELENA time spectrum. Each spectrum was corrected for the background under the energy-gate peaks by subtracting a properly normalized fraction of an ungated matrix. Finally, the five matrices were added together, in order to produce a spectrum collecting a large fraction of the γ decay feeding low-K states. With a similar procedure, a γ-γ spectrum collecting the total decay flow of ^{174}W was sorted by gating on the four lowest transitions of ^{174}W (with spin $\leqslant 10\,\hbar$). As shown in Fig. 2, this latter gating condition strongly selects the population of the yrast band of ^{174}W up to moderately high spins.

Since the intensity of γ rays belonging to high-K bands in ^{174}W is very weak (of the order of ≈1%), a γ-γ spectrum representative of the population of high-K structures was constructed considering only γ's in AGATA in coincidence with delayed transitions, with lifetimes consistent with the known high-K isomers of ^{174}W [14,23]. The quality of the AGATA energy spectra associated with different time gates on the AGATA time spectrum confirms the validity of this time-gating procedure. As shown in Fig. 3, by selecting the delayed part of the AGATA time spectrum [time $\geqslant$ 30 ns, Fig. 3(b)], transitions depopulating the 12^+ and 8^- high-K isomers (indicated by arrows) are largely enhanced, while contributions from prompt γ rays are suppressed (dashed lines), as compared to the intensity distribution associated to prompt events in AGATA [Fig. 3(a)]. In the analysis of the quasicontinuum spectra, the efficiency of the delayed time-gating procedure was enhanced by selecting the isomeric transitions on basis of the HELENA scintillators time spectrum, which has the same structure of the AGATA time spectrum. Therefore, in the case of this time-gating procedure, a background spectrum, properly normalized to the number of time-gating channels, was constructed by selecting the left side of the HELENA time peak, as indicated in the inset of Fig. 3. Finally, the Compton and other uncorrelated background were reduced from the total, low-K, and high-K matrices by the standard COR procedure [35], while all known discrete resolved lines were subtracted by the RADWARE software package [36]. The typical compression to 4 keV/ch was then applied to all spectra before performing the statistical analysis reported in Sec. III.

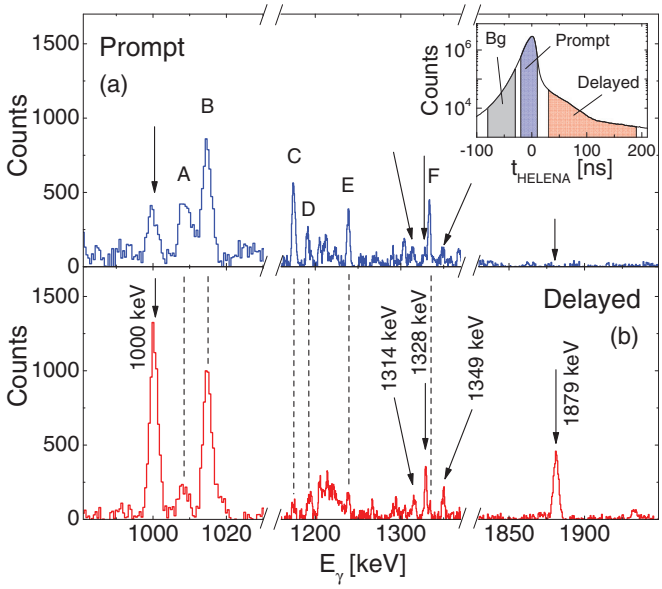


FIG. 3. (Color online) γ energy spectra measured in AGATA, associated to prompt (delayed) γ decays [panels (a) and (b), respectively]. Arrows indicate transitions depopulating the 12^+ and 8^- isomeric states of ^{174}W. Dashed lines point to prompt γ transitions of ^{174}W (A, C, D, and E) or contaminant reaction processes, such as γ decay from ^{27}Al and (n,γ) on ^{73}Ge (B and F) [34]. The prompt ($-20 \leqslant t_{\rm HELENA} \leqslant 20$ ns), delayed ($30 \leqslant t_{\rm HELENA} \leqslant 190$ ns), and background ($-80 \leqslant t_{\rm HELENA} \leqslant -30$ ns) time windows are indicated in the HELENA time spectrum shown in the inset (see text for details).

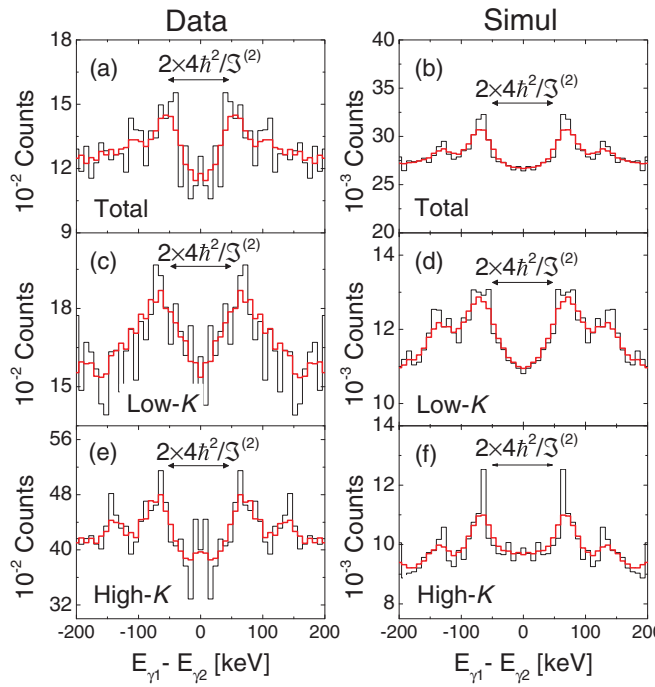


FIG. 4. (Color online) Perpendicular cuts (60-keV wide) of experimental (left) and simulated (right) γ-γ spectra of ^{174}W at the average energy $\langle E_\gamma \rangle = 820$ keV. The matrices collect the total γ-decay flow [panels (a) and (b)] or the γ decay in coincidence with low-K [(c) and (d)] or high-K [(e) and (f)] configurations. In the simulation, low-K (high-K) states correspond to $K \leqslant 6$ ($K > 6$). Arrows indicate the separation between the two innermost ridges. Thin red lines are the first moment (μ_1) spectra, used in the statistical analysis (see text for details).

III. THE EXPERIMENTAL ANALYSIS

Figures 4(a), 4(c), and 4(e) show projections of the total, low-K, and high-K γ-γ matrices, perpendicular to the $E_{\gamma_1} = E_{\gamma_2}$ diagonal, at the average transition energy $\langle E_\gamma \rangle = 820$ keV. The width of the window is $4\hbar^2/\Im^{(2)} = 60$ keV, i.e., the average energy difference between two consecutive transitions in a rotational cascade with dynamic moment of inertia $\Im^{(2)}$. All spectra show the quasicontinuum ridge-valley structure typical of rotational nuclei, with a separation between the two innermost ridges equal to $2 \times 4\hbar^2/\Im^{(2)}$ [20]. In this work we focus on the ridges which are populated by the discrete excited bands close to the yrast line and collect about 6% of the total decay flux of ^{174}W at $I \approx 30$–$40\ \hbar$, as also reported in Ref. [37]. The valley region is instead filled by γ transitions from the warmer rotational regime, where mixing between bands takes place [20]. A quantitative study of the ridges is performed by the fluctuation analysis method (FAM), an *ad hoc* statistical analysis for γ-γ coincidence spectra [24]. It allows us to extract the effective number $N_{\rm path}$ of unresolved discrete bands at least two steps long (named *paths*) through the expression

$$N_{\rm path} = \frac{N_{\rm eve}}{\frac{\mu_2}{\mu_1} - 1} \times \frac{P^{(2)}}{P^{(1)}}, \qquad (1)$$

where $N_{\rm eve}$, μ_1, and μ_2 are the number of recorded events and the first and second moment of the event distribution in an interval $4\hbar^2/\Im^{(2)}$ wide (along the ridge). $P^{(2)}/P^{(1)}$ is a factor taking into account the finite resolution of the detector system. Figure 5 shows the experimental results for the number of discrete bands in ^{174}W as a function of transition energy E_γ. It is found that there are $\sim$35 bands in total [Fig. 5(a)], almost equally distributed between low-K and high-K configurations [Figs. 5(b) and 5(c), respectively], similarly to previous results on ^{163}Er [18,19]. These findings are at the basis of the present experimental study of the hindrance to the $E1$ decay between the entire body of low-K and high-K rotational structures, an investigation which can be performed, in a quantitative way, only through a detailed, microscopic simulation of the γ-decay flow of the warm rotating nucleus of interest, as described in the following Sec. IV.

IV. MONTE CARLO SIMULATION OF THE γ-DECAY FLOW

The interpretation of the data is based on simulation calculations performed by the Monte Carlo program MONTESTELLA [38]. The code simulates the γ-decay flow from the residual entry distribution down to the yrast line, through the competition between statistical $E1$ and collective $E2$ transitions. In the case of ^{174}W, the entry distribution is calculated starting from the fusion cross section of the compound nucleus ^{178}W [39], followed by the evaporation of neutrons, simulated by the Monte Carlo version of the code

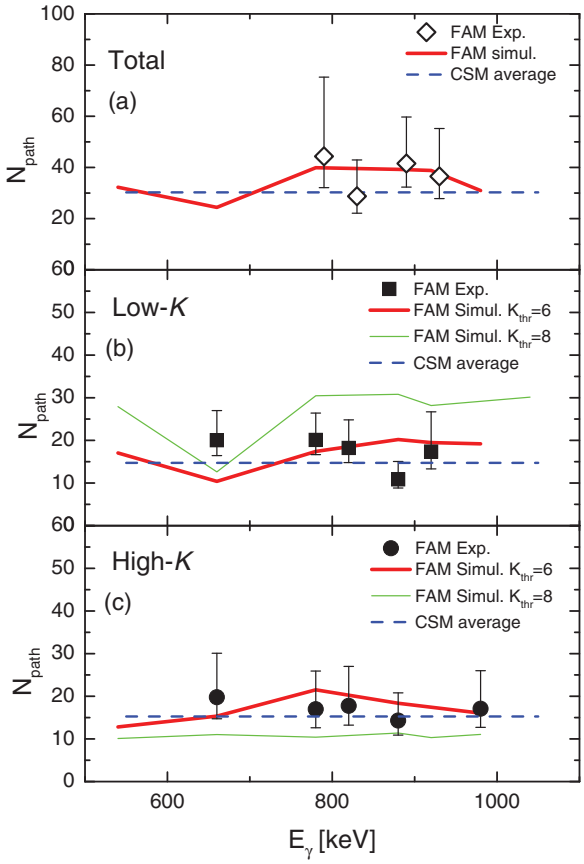


FIG. 5. (Color online) Number of discrete excited bands (*paths*) obtained from the ridge structure analysis of the total (a), low-K (b), and high-K (c) matrices. Symbols refer to experimental data, and thick (thin) solid lines to simulated spectra with the requirement $K_{\rm thr} = 6$ (8). Dashed lines represent the average numbers of discrete excited bands predicted by the cranked shell model with $K_{\rm thr} = 6$ (see text for details).

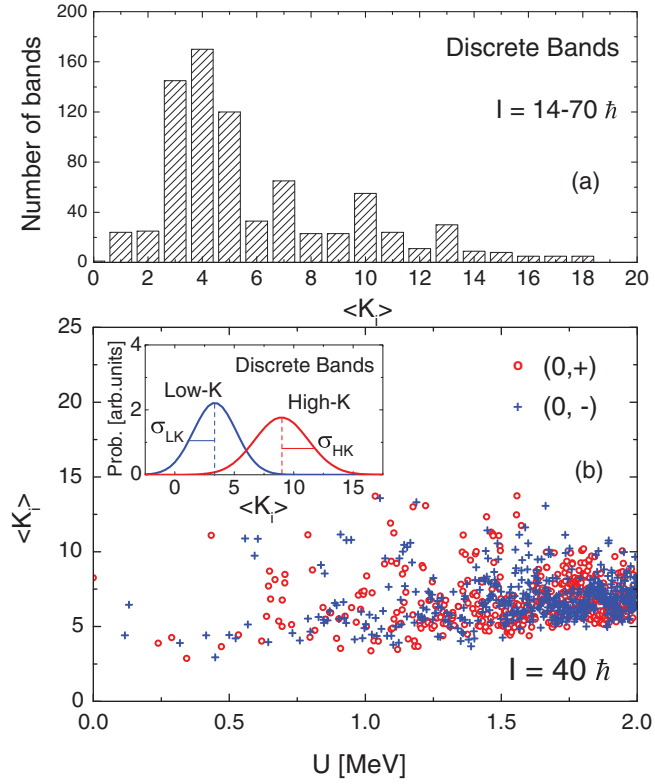


FIG. 6. (Color online) (a) Distribution of average K_i values associated to the discrete excited bands of ^{174}W in the spin range 14–70 $\hbar$, as calculated by the cranking model of Ref. [26], as a function of excitation energy U above yrast. (b) Average K_i values of each positive- (circles) and negative- (crosses) parity state at $I = 40$ $\hbar$, as obtained by the microscopic cranking model. The corresponding, typical intrinsic distributions of K_i values for the low-K and high-K discrete bands (with $\langle K\rangle \leqslant 6$ or >6) are given in the inset by Gaussian shapes (see text for details).

CASCADE [40]. A correction for the experimental multiplicity requirement (F_γ(HELENA) $\geqslant 4$) is also included, leading to a two-dimensional distribution in spin and internal energy with centroids $(I, U) = (52 \pm 10\hbar, 5.5 \pm 2.4$ MeV) for ^{174}W.

The key feature of MONTESTELLA is the use of microscopically calculated levels obtained by the cranked shell model of Ref. [26]. The model assumes a fixed axial deformation ($\epsilon_2 = 0.237$, $\epsilon_4 = 0.02$, and $\gamma = 0.0$ for ^{174}W) and takes into account, in an approximate way, the effect of the K quantum number on the energies of the rotational bands by adding a $-J_z^2/2\Im$ term to the usual cranking Hamiltonian. J_z is the angular momentum operator of the constituent nucleons along the symmetry axis z, while $\Im$ is the kinematic moment of inertia. The calculated rotational bands are then mixed by a two-body residual interaction of surface delta type, with standard interaction strength $V_0 = 27.5/A$ MeV. We notice that Coriolis mixing is essential in order to induce the K mixing, which is in turn amplified by the residual interactions between bands, which by itself would not cause any K violation. One can then evaluate the degree of K mixing associated with each calculated eigenstate $|i\rangle$ at spin I (in the spin range $I = 14$–70 $\hbar$, up to $U \approx 2.5$ MeV), by calculating the average value $\langle K_i\rangle$, $\langle K_i\rangle = \sqrt{\langle i|J_z^2|i\rangle}$ and the standard deviation $\sigma(K_i) = \sigma^2(K_i^2)/(2\langle K_i\rangle)$, where $\sigma^2(K_i^2) = \langle i|J_z^4|i\rangle - \langle i|J_z^2|i\rangle^2$. In addition, the $E2$ decay branch to all possible final states at spin $(I-2)$ is calculated (see Refs. [25,26] for a detailed discussion of the model).

It is found that discrete excited bands of ^{174}W extend up to $\approx$1 MeV above the yrast line, before a progressive fragmentation of the $E2$ decay strength takes place and bands start to mix. In the present context, a band is a sequence of two-consecutive transitions [i.e., a *path*, as defined in connection with Eq. (1)], exhausting more than 71% of the total $E2$ decay strength. This corresponds to less than two final states, as defined by the branching condition $n_{b,i} = \frac{1}{\Sigma_j b_{ij}^2} < 2$, where b_{ij}^2 is the normalized $E2$ strength function from level i with spin I to level j with spin $I-2$. The top panel of Fig. 6 shows the distribution of the average $\langle K_i\rangle$ values for all discrete excited bands microscopically calculated in the spin range $I = 14$–70 $\hbar$. The bottom panel of Fig. 6 gives, as an example, the average $\langle K_i\rangle$ values calculated for each positive- (circles) and negative- (crosses) parity state at $I = 40$ $\hbar$. We have selected those states that belong to a low-K or

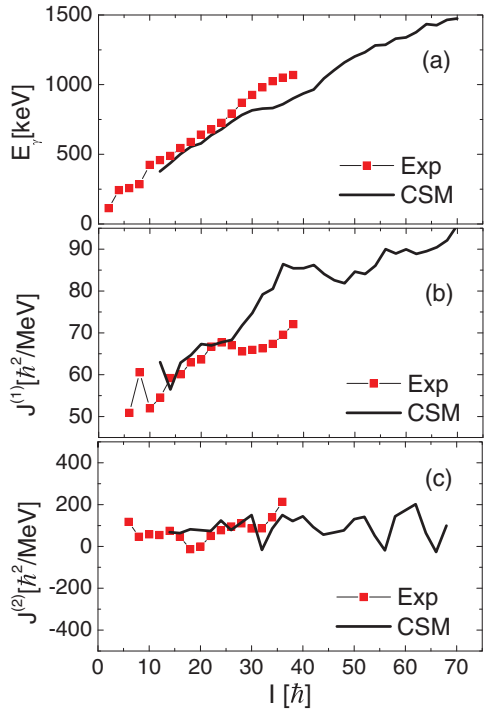


FIG. 7. (Color online) Experimental and microscopically calculated values for transition energies (a), and the first and second moments of inertia [panels (b) and (c), respectively] of the discrete excited bands of ^{174}W, as a function of spins.

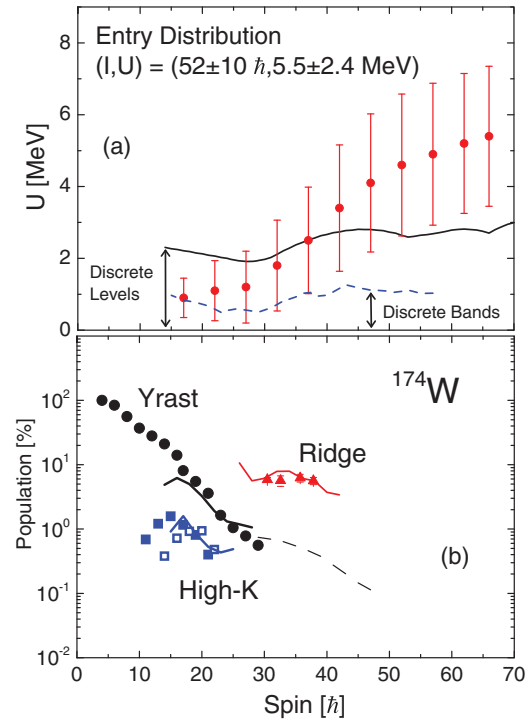


FIG. 8. (Color online) (a) Average internal energy of the γ-decay flow of ^{174}W, as calculated by the MONTESTELLA code for cascades starting from the (I, U) entry distribution given in the legend. The solid/dashed lines denote the regions of internal energies covered by discrete levels/bands. (b) Population intensities, as a function of spins, of the yrast band, high-K bands ($K = 8^-, 12^+$), and total ridge structures extracted from the analysis of experimental (symbols) and simulated (lines) spectra. In the case of the yrast, the solid and dashed lines represent the contribution of the positive- and negative-parity configurations, respectively.

high-K band (with $\langle K\rangle \leqslant 6$ or >6). We have then analyzed their intrinsic distribution of K values. The value of the standard deviation, averaged over the low-K or high-K state distribution, is $\sigma_{\rm LK} = 1.8$ and $\sigma_{\rm HK} = 2.2$. The resulting typical intrinsic distributions of K values for low-K and high-K states, approximated by a Gaussian shape, are shown in the inset of Fig. 6. These are the key ingredients for a proper modeling of K-dependent γ-decay flows; see later discussion.

Finally, Fig. 7 shows a comparison between the experimental and microscopically calculated values for transition energies, and the first and second moments of inertia of the discrete excited bands of ^{174}W, as a function of spins. Apart from specific properties of individual rotational bands, the calculation provides an overall agreement with the experiment, allowing for a quantitative study of average decay properties up into the region of the warm rotation. This is the main feature of the model which, although not adequate for a one-to-one investigation of specific configurations, represents a unique tool for the understanding of nuclear rotation beyond mean field.

In MONTESTELLA the $E1$ transition probability is defined by the strength function of the giant dipole resonance (GDR) built on a prolate nucleus with the same deformation parameters used to produce the microscopic bands (cf. Ref. [19]). The microscopic structure of the quantum states connected by an $E1$ transition is also taken into account by quenching the $E1$ transition probability by a factor $P_{\Delta K}$, depending on the difference in the intrinsic K distributions of the initial and final states (see Fig. 6 and later discussion). Concerning the $E2$ decay probability, this is fully defined through the $E2$ decay strength microscopically calculated for each level up to $U \approx 2.5$ MeV, while above this limit extrapolated values are used [20,38].

Simulated spectra of ^{174}W are shown on the right-hand side of Fig. 4. The low-K (high-K) matrices are built selecting γ cascades with the two lowest spin transitions with $\langle K\rangle \leqslant 6(>6)$. This is consistent with the observation of a large number of rotational structures with $K \leqslant 6$ in ^{174}W [14,23]. It is noted that the overall shape of the simulated spectra reproduces the main features of the experimental distributions rather well, indicating a general agreement between calculated and experimental γ-decay flows. Figure 8 shows, in the top panel, the average internal energy of the decay flow as a function of spin for simulations starting from the entry distribution calculated by CASCADE. It is found that miscoscopically calculated discrete levels are relevant in particular below spin $45\hbar$, where the decay flux rapidly converges towards the region of discrete excited bands [41]. The bottom panel of Fig. 8 gives a comparison between the intensity populations from experiment (symbols) and Monte Carlo calculations (lines) for the yrast band, the high-K bands $K^\pi = 8^-, 12^+$, and the total ridge structure as a function of spin. The overall agreement obtained for each quantity indicates that the Monte Carlo model provides a solid description of the main features

of the γ-decay flow. This is the starting point for further testing of more specific quantities, especially sensitive to the microscopic structure of the excited nuclear levels, as, for example, the number of high-K and low-K rotational bands and their correlation through $E1$ decays.

Figure 5 compares the number of discrete bands extracted from the fluctuation analysis of the ridges of the total, low-K, and high-K experimental and simulated spectra. In all three cases, very good agreement is found between experiment and model predictions, using in the simulation a threshold value $K_{\rm thr} = 6$, between low-K and high-K bands. A higher value of $K_{\rm thr}$ (such as 8) clearly overestimates (underestimates) the experimental number of low-K (high-K) bands obtained by the experimental gating conditions (on energy and time) described in Sec. III. As already pointed out, this agrees with the experimental observation of a large number of low-K bands with $K \leqslant 6$ [14,23]. Moreover, the fact that the fluctuation analysis of the ridge structures of simulated spectra returns the number of discrete excited bands predicted *a priori* by the cranking model (dashed lines in Fig. 5) gives strong reliability to the use of MONTESTELLA to pin down structural properties, associated with the entire body of discrete excited bands, which can only be assessed via a careful simulation of the decay dynamics of the γ flow. More specifically, we here focus on the hindrance to the γ decay associated to large differences of the K quantum number between initial and final states.

The $E1$ decay probability from an initial state in the discrete band region at an energy U_i above yrast is usually taken to be [41]

$$T_{\rm GDR}(E1, U_i) = C \sum_{U_f} f_{\rm GDR}(U_i - U_f) \frac{(U_i - U_f)^3}{\rho(U_i)}, \qquad (2)$$

where $f_{\rm GDR}$ denotes the strength function associated with the tail of the giant dipole resonance. C denotes a phenomenological hindrance factor, introduced to reproduce the measured intensity of the low-lying bands. In dealing with the decay from high-K states to low-K states, we shall modify Eq. (2), introducing an explicit dependence associated with the degree of K forbiddenness. As usual, the probability $P_{\Delta K}$ for decay between two given states having good K quantum numbers K_i and K_f is taken to depend exponentially on the difference $\Delta K = |K_i - K_f|$, namely $P_{\Delta K} = e^{-\frac{\Delta K}{\sigma}}$. Here σ is a phenomenological parameter to be determined. However, in the present case we have to deal with a decay between states which have an intrinsic distribution of K values, assumed to be Gaussian with average values K_i and K_f and variances σ_i and σ_f, determined from the properties of the calculated interacting band. The $E1$ decay probability is then taken to be proportional to

$$P_{\Delta K} = \int dk_1 \frac{e^{-\frac{(k_1 - K_i)^2}{2\sigma_i^2}}}{\sqrt{2\pi\sigma_i^2}} \int dk_2 \frac{e^{-\frac{(k_2 - K_f)^2}{2\sigma_f^2}}}{\sqrt{2\pi\sigma_f^2}} e^{-\frac{|k_1 - k_2|}{\sigma}}. \qquad (3)$$

The probability for $E1$ decay from an initial state i to a final state f is then calculatedby multiplying the GDR strength $f_{\rm GDR}(U_i - U_f)$ by $P_{\Delta K}$ in Eq. (2).

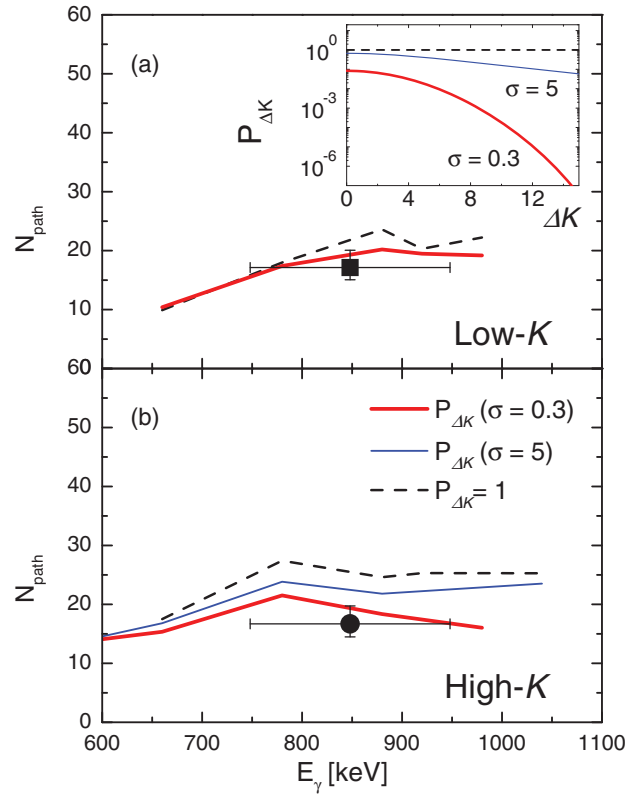


FIG. 9. (Color online) Comparison between the number of paths extracted from experimental data (symbols) and simulated spectra (lines) for low-K (a) and high-K (b) ridge structures. Simulations are performed for values of $\sigma = 0.3$, 5, and >500, corresponding to the $P_{\Delta K}$ quenching factors shown in the inset (with $\sigma_i = \sigma_f = 2$, as in the case of the discrete excited bands). Experimental points have error bars on E_γ representing the energy region used for the statistical fluctuation analysis.

In the spin region $I = 20$–$50\hbar$, the discrete excited bands of ^{174}W (extending up to $\approx$1 MeV above yrast) have K-quantum-number distributions with centroids around $K \approx 3$ and 8.6 for low-K and high-K structures, respectively, with similar standard deviations ($\sigma_i \approx \sigma_f \approx 2$, cf. Fig. 6 and related discussion). By using the value $\sigma \approx 0.3$, a strong quenching is obtained in the $E1$ decay probability of the order of 10^{-2} for $\Delta K \approx 6$. On the contrary, if the σ parameter is larger than 1 the quenching factor $P_{\Delta K}$ is close to 1, even for large ΔK values [as shown in the inset of Fig. 9(a)].

Figures 9(a) and 9(b) show the sensitivity of the number $N_{\rm path}$ of discrete bands, extracted from the analysis of simulated low-K and high-K spectra, to the σ parameter of $P_{\Delta K}$. Simulations are performed for the three values $\sigma = 0.3$, 5, 500 (the latter corresponding to $P_{\Delta K} \approx 1$), adjusting C so as to reproduce the observed intensisites of low-lying bands. The results are compared to the experimental number of discrete bands obtained by considering a wide energy interval along the ridge structures of the low-K and high-K matrix to minimize statistical errors. While the number of low-K bands is rather insensitive to the choice of σ, a larger sensitivity is observed in the number of high-K discrete excited bands. As shown by the dashed (thin) line in Fig. 9(b), by neglecting

the $P_{\Delta K}$ quenching in the $E1$ decay (or by using a modest correction), a too-large number of high-K bands (more than 20) is obtained, even larger than the number of high-K bands ($\approx$15) calculated by the cranked shell model [dashed line in Fig. 5(c)]. The best results are obtained with $\sigma = 0.3$, and this value was used in Fig. 5.

It is then possible to obtain an estimate of the average hindrance of $E1$ decay between high-K and low-K bands. The average reduced hindrance f_ν is calculated starting from the definition $f_\nu = (\frac{T(E1)_W}{T(E1)_\gamma})^{1/\nu}$ [7], with $T(E1)_W$ being the $E1$ decay probability in Weisskopf units and $T(E1)_\gamma$ the effective $E1$ decay probability used in the simulation code [19], obtained by multiplying $f_{\rm GDR}$ by $P_{\Delta K}$ in Eq. (2). The entire body of discrete excited bands, microscopically calculated between the yrast line and the onset of the band mixing regime (at $U \approx 1$ MeV), has been considered and divided into the spin intervals $I = 30 \pm 5\hbar$ and $45 \pm 10\hbar$. In addition, the spin region around $30\hbar$ (where the γ flow well populates the discrete excited bands) has been further subdivided into two internal energy intervals. For each group of states, the average transition energy E_γ of the $E1$ transitions between the high-K ($K > 6$) and low-K ($K \leqslant 6$) states has been determined by averaging over all possible simulated $E1$ decays. For the evaluation of $P_{\Delta K}$, sets of high-K and low-K states have been considered separately in order to extract the centroid of the average K values (K_i and K_f) and the corresponding standard deviation (σ_i and σ_f) given by the cranked shell model and needed to evaluate $P_{\Delta K}$ [cf. Eq. (3) and Fig. 6, as an example]. The initial (final) state is always assumed to be of high-K (low-K) nature.

The results are shown by filled circles in Fig. 10. The last point at $U = 1.15$ MeV refers to the analysis of microscopic levels extending into the band mixing region, where the decay flow becomes fragmented over several final states. While the error bars on the energy scale refer to the interval considered for the averaging over the excited levels, the errors on f_ν are dominated by the uncertainty on the σ parameter of $P_{\Delta K}$, calculated considering the experimental error on the number of high-K bands (see Fig. 9). By using $\sigma = 5$ [a value which does not reproduce the experimental number of high-K bands, cf. Fig. 9(b)] lower values of f_ν are instead obtained of the order of 20–30 and with no dependence on excitation energy.

Our results are compared in Fig. 10 with the reduced decay hindrances f_ν, obtained from high-K isomers in the mass region $A \approx 160$–180 as a function of internal energy [9]. The solid (dotted) line represents the f_ν curve for $\nu = 4$ ($\nu = 3$), as follows from a K-mixing model which assumes the level density as mainly responsible for the weakening of K-forbidden transition rates with U [16]. It is seen that our values are similar to those found in K isomer decay from discrete states at comparable excitation energy and follow the same trend. This suggests that K mixing due to temperature effects may play a leading role in the progressive weakening of the K quantum number already at rather low internal energy, i.e., in the onset region of the band mixing regime, here probed by the decay properties of the entire body of discrete excited bands. These findings represent an important complement to those of discrete spectroscopy, although for a more complete

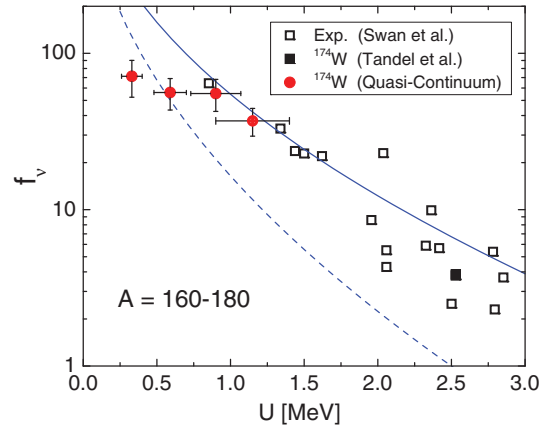


FIG. 10. (Color online) Reduced hindrance f_ν, as a function of internal energy U, for nuclei in the mass region $A \approx 160$–180. Open squares are experimental data from Ref. [9], with the full square representing the reduced hindrance factor reported in Ref. [14] for the 12^+ isomer of ^{174}W. Full red circles are obtained from the present quasicontinuum analysis of the quenching of the $E1$ decay between discrete excited bands of ^{174}W, using $\sigma = 0.3$ in the calculation of $P_{\Delta K}$ [cf. Eq. (3)]. The last point at $U = 1.15$ MeV refers to the analysis of microscopic levels extending into the damping region. The solid (dotted) line represents the f_ν curve for $\nu = 4$ ($\nu = 3$), calculated with the analytical model of Ref. [16] (see text for details).

comparison with the case of isomer decay, a similar type of study should be pursued all the way up into the higher excitation energy regime of strongly interacting bands. Such a detailed study would require not only high statistics and high-quality data but also a more microscopic treatment of the $E1$ decay between the high-K and low-K configurations, so far parametrized in a phenomenological fashion.

V. CONCLUSION

In summary, the present work reports on the experimental investigation of the warm rotational motion in ^{174}W, performed with the AGATA Demonstrator array. The focus is on the quasicontinuum ridge structures of γ-γ coincidence matrices, collecting the decay flow based on low-K and high-K intrinsic configurations. By fluctuation analysis techniques, a similar number of low-K and high-K discrete excited bands ($\approx$15) is obtained and compared to simulations of the γ decay, based on microscopic cranked shell model calculations at finite temperature. This offers a unique opportunity to probe the properties of the γ-decay flow for the entire body of discrete excited bands. Agreement between data and model predictions is obtained only by strongly hindering the $E1$ decay between low-K and high-K bands. Moreover, a dependence on internal energy is deduced, with a trend in accordance with spectroscopic studies of K isomers in the same mass region. The present results suggest that a K-mixing process due to temperature effects plays an important role already at rather low excitation energy, namely in the onset region of band mixing, here probed by a global analysis of decay properties of the entire body of discrete excited bands. This represents a step forward in the understanding of the basic

rules governing the isomeric systems and calls for similar, additional investigation at higher excitation energies, where the erosion of the K quantum number becomes even more severe.

ACKNOWLEDGMENTS

The present work is the outcome of one of the first experiments performed at LNL with the AGATA Demonstrator array. This was possible through the technical and scientific effort of a large group of people, who contributed in various ways to the success of the first implementation of the AGATA array, as demonstrated by the long list of coauthors. The authors are grateful to the accelerator team of LNL for the high quality of the beam delivered during the experiment and their constant support. Discussions with T. Døssing and S. Åberg are also gratefully acknowledged. This work was supported by the Italian Istituto Nazionale di Fisica Nucleare. Support was also given by the Generalitat Valenciana (Spain) under Grant No. PROMETEO/2010/101, by MINECO (Spain) under Grants No. AIC-D-2011-0746 and No. FPA2011-29854, by the Polish National Center of Science (Grant No. 2011/03/B/ST2/01894), and by the Polish Ministry of Science and Higher Education (Grant No. DPN/N190/AGATA/2009).

[1] P. M. Walker and G. D. Dracoulis, Nature **399**, 35 (1999).
[2] P. M. Walker and J. J. Carroll, Phys. Today **58**(6), 39 (2005).
[3] G. D. Dracoulis, Phys. Scr. T **152**, 014015 (2013).
[4] S. Frauendorf, Rev. Mod. Phys. **73**, 463 (2001).
[5] K. Matsuyanagi, M. Matsuo, T. Nakatsukasa, N. Hinoara, and K. Sato, J. Phys. G: Nucl. Part. Phys. **37**, 064018 (2010).
[6] K. Heyde and J. L. Wood, Rev. Mod. Phys. **83**, 1467 (2011).
[7] K. E. G. Loebner, Phys. Lett. B **26**, 369 (1968).
[8] A. Bohr and B. R. Mottelson, *Nuclear Structure* (Benajamin, London, 1975), Vol. II.
[9] T. P. D. Swan *et al.*, Phys. Rev. C **86**, 044307 (2012).
[10] P. Chowdhury *et al.*, Nucl. Phys. A **485**, 136 (1988).
[11] J. Pedersen *et al.*, Phys. Rev. Lett. **54**, 306 (1985).
[12] T. Bengtsson, R. A. Broglia, E. Vigezzi, F. Barranco, F. Donau, and J. Y. Zhang, Phys. Rev. Lett. **62**, 2448 (1989).
[13] K. Narimatsu, Y. R. Shimizu, and T. Shizuma, Nucl. Phys. A **601**, 69 (1996).
[14] S. K. Tandel *et al.*, Phys. Rev. C **73**, 044306 (2006).
[15] S. Frauendorf, *Proceedings of the International Conference on the Future of Nuclear Spectroscopy, Crete, 27 June–3 July 1993*, edited by W. Gelletly, C. A. Kalfas, R. Vlastou, S. Harissopulos, and D. Loukas (I.N.P., National Center for Scientific Research Demokritos, Athens, Greece, 1994).
[16] P. M. Walker *et al.*, Phys. Lett. B **408**, 42 (1997).
[17] P. Bosetti *et al.*, Phys. Rev. Lett. **76**, 1204 (1996).
[18] G. Benzoni *et al.*, Phys. Lett. B **615**, 160 (2005).
[19] S. Leoni *et al.*, Phys. Rev. C **72**, 034307 (2005).
[20] A. Bracco *et al.*, Rep. Prog. Phys. **65**, 299 (2002).
[21] S. Akkoyun *et al.*, Nucl. Instrum. Methods A **668**, 26 (2012).
[22] A. Gadea *et al.*, Nucl. Instrum. Methods A **654**, 88 (2011).
[23] S. K. Tandel *et al.*, Phys. Rev. C **77**, 024313 (2008).
[24] T. Døssing *et al.*, Phys. Rep **268**, 1 (1996).
[25] M. Matsuo *et al.*, Nucl. Phys. A **620**, 296 (1997).
[26] M. Matsuo *et al.*, Nucl. Phys. A **736**, 223 (2004).
[27] S. Frattini *et al.*, Phys. Rev. Lett. **83**, 5234 (1999).
[28] S. Leoni *et al.*, Phys. Rev. Lett. **93**, 022501 (2004).
[29] S. Leoni *et al.*, Phys. Rev. Lett. **101**, 142502 (2008).
[30] S. Leoni *et al.*, Phys. Rev. C **79**, 064306 (2009).
[31] S. Leoni *et al.*, Phys. Rev. C **79**, 064307 (2009).
[32] O. B. Tarasov and D. Bazin, Nucl. Instrum. Methods B **204**, 174 (2003).
[33] T. Kroll and D. Bazzacco, Nucl. Instrum. Methods A **565**, 691 (2006).
[34] J. Chao, Appl. Radiat. Isot. **44**, 605 (1993).
[35] C. Ellegaard *et al.*, Phys. Rev. Lett. **48**, 670 (1982).
[36] D. C. Radford, Nucl. Instrum. Methods A **361**, 297 (1995).
[37] M. Cromaz *et al.*, Phys. Rev. C **54**, 2055 (1996).
[38] A. Bracco *et al.*, Phys. Rev. Lett. **76**, 4484 (1996).
[39] A. Winther, Nucl. Phys. A **594**, 203 (1995).
[40] F. Pulhofer, Nucl. Phys. A **280**, 267 (1977).
[41] T. Døssing and E. Vigezzi, Nucl. Phys. A **587**, 13 (1995).